Ref: OUNP-89-18

A MEASUREMENT OF THE PROTON STRUCTURE FUNCTIONS FROM NEUTRINO-HYDROGEN AND ANTINEUTRINO-HYDROGEN CHARGED-CURRENT INTERACTIONS

Birmingham–CERN–Imperial College–München (MPI)–
Oxford–University College London–Collaboration

NUCLEAR PHYSICS LABORATORY

DOMINUS ILLUMINATIO MEA

OXFORD UNIVERSITY

21st June 1989

A MEASUREMENT OF THE PROTON STRUCTURE FUNCTIONS FROM NEUTRINO-HYDROGEN AND ANTINEUTRINO-HYDROGEN CHARGED-CURRENT INTERACTIONS

Birmingham–CERN–Imperial College–München (MPI)–Oxford–University College London–Collaboration

G.T. Jones, R.W.L. Jones(*)(+), B.W. Kennedy(*)(†), S.W. O'Neale
Department of Physics, University of Birmingham, Birmingham, UK

H. Klein, D.R.O. Morrison, P. Schmid and H. Wachsmuth
CERN, European Organization for Nuclear Research, Geneva, Switzerland

F. Hamisi, D.B. Miller, M.M. Mobayyen and S. Wainstein(*)
Department of Physics, Imperial College, London, UK

M. Aderholz, D. Hantke, E. Hoffmann, U.F. Katz, J. Kern, N. Schmitz and W. Wittek
Max-Planck Institut für Physik und Astrophysik, München, Germany

G. Corrigan, G. Myatt, D. Radojicic, P.N. Shotton(*) and S.J. Towers(*)
Department of Nuclear Physics, Oxford, UK

F.W. Bullock and S. Burke(*)(‡)
Department of Physics and Astronomy, University College London, London, UK

To be published in *Zeitschrift für Physik C*

ABSTRACT

Within the framework of the quark-parton model, the quark and anti-quark structure functions of the proton have been measured by fitting them to the distributions of the events in the Bjorken y variable. The data used form the largest sample of neutrino and antineutrino interactions on a pure hydrogen target available, and come from exposures of BEBC to the CERN wide band neutrino and antineutrino beams. It is found that the ratio d_v/u_v of valence quark distributions falls with increasing Bjorken x. In the context of the quark-parton model the results constrain the isospin composition of the accompanying diquark system. Models involving scattering from diquarks are in disagreement with the data.

(*) Supported by an SERC grant.

(†) Present address: University College London, London, UK.

(‡) Present address: Rutherford Appleton Laboratory, Chilton, Didcot, UK.

(+) Present address: Queen Mary College, London, UK.

1. INTRODUCTION

This paper presents measurements of the proton charged-current structure functions. The data come from the WA21 experiment, in which the Big European Bubble Chamber (BEBC), filled with liquid hydrogen, was exposed to the wide band neutrino and antineutrino beams generated by 400 GeV protons from the CERN SPS.

Measurements using neutrinos (antineutrinos) as probes of the nucleon structure are important because only neutrino experiments have the ability to measure the momentum distributions of the different quark flavours separately, and to distinguish quarks from antiquarks. Measurements on a hydrogen target have become increasingly important since results from the EMC [1] experiment and SLAC [2] indicate that the free nucleon structure cannot be simply inferred from measurements made on nuclear targets.

2. THE EXPERIMENT

2.1 The neutrino and antineutrino beams

Protons of energy 400 GeV (350 GeV for the neutrino data taken in 1977) extracted from the CERN SPS were incident on a beryllium target, and the secondary hadrons (mainly pions and kaons) were then sign-selected by a system of magnetic horns. Following the horns was a 300 m long evacuated tunnel in which the secondary hadrons were allowed to decay, and 400 m of iron and earth shielding. The energy spectrum of the neutrino beam was inferred from the associated muon flux measured by solid state detectors [3] in five gaps in the iron shielding.

The absolute normalization of the neutrino flux was obtained from the total cross sections, determined [4] using data from this experiment and the WA59 BEBC neon experiment, together with the neon cross sections measured by the WA47 Collaboration using the narrow band neutrino (antineutrino) beam.

2.2 The apparatus

The detector used in this experiment was the bubble chamber BEBC filled with liquid hydrogen, equipped with a two-plane external muon identifier (EMI) [5] throughout the data taking. For the latter part of the experiment BEBC was also equipped with a cylindrical array of single wire proportional tubes, referred to as the Internal Picket Fence (IPF) [6], placed around the chamber in order to record position and time information for all charged particles entering or leaving BEBC.

3. METHOD OF ANALYSIS

The νp and $\bar{\nu} p$ charged current differential cross sections are defined in terms of the three dimensionless structure functions $F_i^{\nu,\bar{\nu}}$, $i = 1,2,3$:

$$\frac{d^2\sigma^{\nu,\bar{\nu}}}{dx dy} = \frac{G^2 ME}{\pi} \frac{M_W^4}{(Q^2 + M_W^2)^2} \left\{ \frac{y^2}{2} 2xF_1^{\nu,\bar{\nu}} + \left(1 - y - \frac{Mxy}{2E}\right) F_2^{\nu,\bar{\nu}} \pm y(1 - \frac{y}{2})xF_3^{\nu,\bar{\nu}} \right\} \quad (1)$$

where

$F_i^{\nu,\bar{\nu}} = F_i^{\nu,\bar{\nu}}(x, Q^2)$,
E = the neutrino (antineutrino) energy in the lab. system,
M = the nucleon mass,
Q^2 = the four-momentum transfer squared,
ν = the energy transfer $E - E_\mu$ in the lab. system,
y $= \nu/E$,
x $= Q^2/2M\nu$,
G = the Fermi constant,
M_W = the mass of the W boson

and the upper and lower sign is for a neutrino beam and an antineutrino beam, respectively. We define two structure functions $q(x,Q^2)$ and $\bar{q}(x,Q^2)$ in terms of F_1 and F_3 such that

$$2xF_1(x,Q^2) = 2x\{q(x,Q^2) + \bar{q}(x,Q^2)\} \tag{2}$$
$$xF_3(x,Q^2) = 2x\{q(x,Q^2) - \bar{q}(x,Q^2)\}, \tag{3}$$

where in the framework of the quark-parton model $xq^{\nu} = x(d+s)$, $x\bar{q}^{\nu} = x(\bar{u}+\bar{c})$ for neutrino scattering, and $xq^{\bar{\nu}} = x(u+c)$, $x\bar{q}^{\bar{\nu}} = x(\bar{d}+\bar{s})$ for antineutrino scattering, are the fractions of the proton momentum carried by the quarks and antiquarks, of flavours u, d, etc.

The structure function F_2 is then defined in terms of q, $\bar{q}$ and R, where R is the ratio of the cross sections for absorption of longitudinally and transversely polarized W bosons.

$$F_2 = \frac{1+R}{1+Q^2/\nu^2}2x(q+\bar{q}). \tag{4}$$

Rewriting the differential cross section in terms of q, $\bar{q}$ and R we thus have

$$\frac{d^2\sigma^{\nu,\bar{\nu}}}{dxdy} = \frac{2G^2MEx}{\pi}\frac{M_W^4}{(Q^2+M_W^2)^2}\left\{q^{\nu,\bar{\nu}}(x,Q^2)\left(\frac{y^2}{2} \pm (y-\frac{y^2}{2})+\eta\right)\right.$$
$$\left. + \bar{q}^{\nu,\bar{\nu}}(x,Q^2)\left(\frac{y^2}{2} \mp (y-\frac{y^2}{2})+\eta\right)\right\} \tag{5}$$

where

$$\eta = \left(1-y-\frac{Mxy}{2E}\right)\frac{1+R(x,Q^2)}{1+Q^2/\nu^2}.$$

In the Bjorken limit

$$\lim_{\substack{Q^2\to\infty \\ \nu\to\infty}},\ x \text{ fixed} \quad R = 0$$
$$\lim_{\substack{Q^2\to\infty \\ \nu\to\infty}},\ x \text{ fixed} \quad \eta = (1-y)$$

the formulae for the differential cross sections become

$$\frac{d^2\sigma^{\nu}}{dxdy} = \frac{2G^2MEx}{\pi}\frac{M_W^4}{(Q^2+M_W^2)^2}\{q^{\nu}(x,Q^2) + \bar{q}^{\nu}(x,Q^2)(1-y)^2\} \tag{6}$$

for a neutrino beam, and

$$\frac{d^2\sigma^{\bar{\nu}}}{dxdy} = \frac{2G^2MEx}{\pi}\frac{M_W^4}{(Q^2+M_W^2)^2}\{q^{\bar{\nu}}(x,Q^2)(1-y)^2 + \bar{q}^{\bar{\nu}}(x,Q^2)\} \tag{7}$$

for an antineutrino beam.

From equation (7) we see that antineutrino scattering is dominated at large y by the antiquark sea $x(\bar{d}+\bar{s})$, and hence this structure function may be extracted from a fit to the antineutrino y distribution. However, it is not practical to extract the corresponding antiquark structure function in neutrino scattering, $x(\bar{u}+\bar{c})$, by this method because this structure function is nowhere dominant in the y distribution (see equation (6)).

We have insufficient data to measure $q(x,Q^2)$, $\bar{q}(x,Q^2)$ and $R(x,Q^2)$; we are forced to assume some form for the Q^2 dependence of the structure functions, and for

$R(x, Q^2)$, which is poorly determined experimentally. We have assumed that the Q^2 dependence of the structure functions is adequately described by the formula

$$q(x, Q^2) = q(x, Q_0^2)\left(\frac{Q^2}{Q_0^2}\right)^{\alpha(x)} \tag{8}$$

with a similar expression for the antiquark structure function, where $\alpha(x)$ varies from 0.14 at $x = 0$ to -0.20 at $x = 0.7$ and is consistent with QCD and recent deep inelastic scattering data [7]. $R(x, Q^2)$ is assumed to be a function of x, independent of Q^2, for the Q^2 range of our experiment. The values taken for $R(x)$ are discussed in section 5.

The number of events in the i^{th} bin of x and the j^{th} bin of y is then

$$\begin{aligned} N_{ij}^{\nu,\bar{\nu}} =& n_t \int_{x_1}^{x_2} dx \int_{y_1}^{y_2} dy \int_{E_1}^{E_2} dE \frac{d^2\sigma^{\nu,\bar{\nu}}}{dxdy}\phi^{\nu,\bar{\nu}}(E) \\ =& \frac{n_t G^2}{\pi} \int_{x_1}^{x_2} dx \int_{y_1}^{y_2} dy \int_{Q_1^2}^{Q_2^2} dQ^2 \left\{ xq^{\nu,\bar{\nu}}(x, Q_0^2)\left(\frac{y^2}{2} \pm (y - \frac{y^2}{2}) + \eta\right) + \right. \end{aligned}$$

$$\left. x\bar{q}^{\nu,\bar{\nu}}(x, Q_0^2)\left(\frac{y^2}{2} \mp (y - \frac{y^2}{2}) + \eta\right)\right\} \phi^{\nu,\bar{\nu}}(E) \frac{M_W^4}{(Q^2 + M_W^2)^2} \frac{Q^2}{2Mx^2y^2}\left(\frac{Q^2}{Q_0^2}\right)^{\alpha(x)}, \tag{9}$$

where the variable in E the flux integral can be changed to Q^2 using $E = Q^2/2Mxy$. The i^{th} bin of x is from x_1 to x_2, the j^{th} bin of y is from y_1 to y_2, and Q_1^2 to Q_2^2 is the kinematically allowed range of the variable Q^2 for given $x_1 \leq x \leq x_2$, $y_1 \leq y \leq y_2$ and $E_1 \leq E \leq E_2$, where E_1 and E_2 are the minimum and maximum neutrino energies (see section 4). n_t is the number of protons in the fiducial volume of the target, and $\phi^{\nu,\bar{\nu}}(E)$ is the neutrino (antineutrino) flux spectrum.

Assuming that $xq(x, Q_0^2)$ and $x\bar{q}(x, Q_0^2)$ are constant within each bin of x and y these structure functions may be evaluated by fitting the expression

$$N_{ij}^{\nu,\bar{\nu}} = I_{ij}^{\nu,\bar{\nu}} xq^{\nu,\bar{\nu}}(x, Q_0^2) + \bar{I}_{ij}^{\nu,\bar{\nu}} x\bar{q}^{\nu,\bar{\nu}}(x, Q_0^2) \tag{10}$$

where $I_{ij}^{\nu,\bar{\nu}}$ and $\bar{I}_{ij}^{\nu,\bar{\nu}}$ are the values of appropriate integrals over x, y, Q^2 for each bin of x and y.

4. EVENT SELECTION AND CORRECTIONS

In order to determine the event distributions the following selection criteria were applied to all events:

(a) The vertex of the event was required to lie within the fiducial volume of 19 m^3 used for the experiment.

(b) The event was required to occur during a period for which the neutrino beam was stable. Beam constancy was ensured with the aid of the array of muon flux detectors distributed throughout the shielding. All pulses for which the shape of the muon flux distribution was not in accord with a chosen standard were eliminated from the analysis.

(c) The event was required to have a final state muon of correct charge (i.e. μ^- for neutrino scattering and μ^+ for antineutrino scattering), and momentum $p_\mu > 4$ GeV/c, identified by both planes of the EMI. The performance of each wire in the EMI was monitored regularly using cosmic rays. The geometrical acceptance of the EMI was over 98% for muons with $p_\mu > 10$ GeV/c, falling to 70% for $p_\mu = 4$ GeV/c. The efficiency for detecting muons which lay within the acceptance (the electronic efficiency) was calculated separately for each data set and averaged $95 \pm 2\%$.

To determine the neutrino (antineutrino) energy of each event the final state charged particle tracks were measured, and the energy loss due to the undetected neutral particles was corrected for by a method involving total transverse momentum balance about the beam direction [8]. The estimated neutrino energy was required to be between 20 GeV and 300 GeV, and Q^2 was required to be greater than 2 $(\mathrm{GeV/c})^2$ in order to remove data in the elastic and resonance region, and hence ensure the validity of the parton model. To check that this requirement was sufficiently stringent the structure functions were recalculated using different Q^2 cuts. For $Q^2 > 2$ $(\mathrm{GeV/c})^2$ the change in the values of the structure functions for different Q^2 cuts was negligible, but for $Q^2 < 2$ $(\mathrm{GeV/c})^2$ the values change by an amount larger than the statistical uncertainty.

The resulting samples of ~ 11800 νp and ~ 7400 $\bar{\nu} p$ events were binned in x and y, and corrected for the EMI acceptance and electronic efficiency. The corrections for the geometrical acceptance were bin dependent, and on average were 4% for the νp case and 2% for the $\bar{\nu} p$ case. The background from neutral current events misidentified as charged current events due to hadron punch-through, pion decay and random associations of hits in the EMI was also corrected for. This correction involved less than 1% of the events.

The scanning efficiency was calculated as a function of the charged multiplicity of the event separately for each data set on the basis of a second scan of all the film, and, for the data for which IPF information was available, of a scan for events predicted by correlating hits in the IPF and both planes of the EMI. For events with 3 prongs the average scanning efficiency was $(0.93 \pm .02)$ and for events with ≥ 5 prongs $(0.99 \pm .01)$. The reactions $\bar{\nu} p \rightarrow \mu^+ +$ neutrals (the so-called one-prong topology) had a low scanning efficiency, and the method of transverse momentum balance used to estimate the antineutrino energy fails for events of this type. Consequently these events were removed from the data sample and a Monte Carlo computer programme [9] written to simulate the experiment was used to calculate correction factors to be applied to each bin to account for the events of this topology. This correction becomes large at large x and small y, but falls rapidly for decreasing x, and for the majority of bins is less than 10%.

For both the νp and $\bar{\nu} p$ samples the programme was also used to find correction factors to account for the uncertainties in energy determination, track measurement errors and particle misidentification ("smearing effects"), and radiative processes. The size of the smearing correction was on average 15%, and was less than 55% for any $x < 0.7$; at larger x the correction factors become larger, and the data are less reliable. Corrections for radiative processes were calculated following de Rujula *et al.* [10].

The effects of thresholds for the production of charmed quarks in the final state were calculated using slow rescaling [11] and a charmed quark mass of 1.5 $\mathrm{GeV/c^2}$. The corrections for these effects were found to be negligible.

5. THE RESULTS

The values assumed for $R(x)$ and $\alpha(x)$ are given in table 1. These values are consistent [7] with the predictions of QCD, and with recent experimental data. The systematic error due to $R(x)$ was estimated by increasing each value by 25% and recalculating the structure functions.

The point-to-point systematic error due to the assumed value of α was estimated by the shift in the structure functions when α is changed by ± 0.05. This change allows for the dependence of α on the different quark flavours and differences between the dependences of quarks and antiquarks.

For $x > 0.3$ it is known from high statistics measurements [7] on nuclear targets that the antiquark structure functions are very small and it is reasonable to set them to zero in the present analysis. The values of the structure functions $xq^{\nu}(x, Q_0^2)$, $xq^{\bar{\nu}}(x, Q_0^2)$, $x\bar{q}^{\bar{\nu}}(x, Q_0^2)$ as functions of x, extracted at the mean Q^2 of the data ($Q_0^2 = 14.2$ (GeV/c)^2 for the neutrino case, $Q_0^2 = 8.6$ (GeV/c)^2 for the antineutrino case), are given in tables 2–4. The statistical errors are shown and the point-to-point systematic shifts in the measurement of the structure functions due to the uncertainties in the flux shape, the Q^2 interpolation prescription, the value of $R(x)$, and the smearing factors, which were estimated using another Monte Carlo programme with a different model for hadron generation. The signs given in the tables indicate whether the structure function increases (+) or decreases (−) when either α or $R(x)$ is increased. It should be noted that, to the extent that $\alpha(x)$ and $R(x)$ can be predicted by perturbative QCD, their values are highly correlated and that a combination in quadrature of their errors might not be appropriate in this case. The structure function $x\bar{q}^{\nu}$ is left as a free parameter for $x < 0.3$, but the data are insufficient to allow its determination. The whole range of y is used at each x. In addition to the quoted errors there is a systematic uncertainty in the flux normalizations. This was found to be ±6%, calculated from the measured total cross sections [4].

The systematic errors due to the scanning efficiency for low multiplicity events were estimated by increasing the fraction of events with low prong topologies by 10%, but the changes to the structure functions were found to be negligible.

A comparison can be made of our results with published data from experiments on hydrogen [12] and deuterium [13]. Care must be taken to allow for the differences in the values of Q^2 at which the structure functions have been determined. Furthermore all experiments base their absolute normalizations on assumed values of the total neutrino and antineutrino cross sections and these differ considerably between experiments. When these facts are taken into account the present structure functions agree within their statistical and systematic errors with the previously published data over the whole x range.

The valence quark structure functions d_v and u_v can be defined by the relations $d_v = q^{\nu} - \bar{q}^{\bar{\nu}}$ and $u_v = q^{\bar{\nu}} - \bar{q}^{\nu}$. Values for these structure functions, interpolated at $Q^2 = 11.5$ (GeV/c)^2, are shown in table 5 with their statistical and systematic errors. The ratio d_v/u_v is a measure of the violation of SU(6) symmetry in the structure functions and has been studied in previous experiments. Our results are shown in table 5 and in figure 1 as a function of x. They constitute the most accurate measurements of this ratio so far published and are consistent with previous results [14]. It can be seen that at low x the ratio is compatible with the simple quark-parton model expectation of 0.5. However, at larger x the ratio falls progressively below this value indicating dominance of the majority quark flavour.

Using isospin arguments Field and Feynman [15] predicted that d_v/u_v should tend to zero as $x \to 1$. The data are clearly compatible with this. However, Farrar and Jackson [16] have argued that at large x values the struck quark should have the helicity of the target proton. Using the SU(6) description of the proton, it then follows that the relative probability of striking a d or u quark is $^1/_5$. Results at larger x values would be needed to make a definitive comparison with this prediction.

Close [17] and Carlitz [18] have represented the SU(6) violation in terms of a parameter a, where

$$A_1/A_0 = a(1-x)$$

and A_1 and A_0 are the probabilities for the spectator diquark system to have isospin 1 or 0 respectively. As can be seen in figure 1, the data favour values of a near its lower limit of unity.

Recently Close and Thomas [19] have published calculations of the nucleon structure function based on the mass shifts introduced by the colour hyperfine interaction. Interpreting their results for F_2^{en}/F_2^{ep} in terms of the valence quark distributions for $x > 0.3$ (where sea quarks may be neglected) it can be seen in figure 1 that their calculation predicts a more rapid variation with x than is found in the data.

Various models have been proposed to account for the scaling violations in deep inelastic reactions in terms of scattering from diquarks. A simple calculation of Close and Roberts [20], based on a model of Donnachie and Landshoff [21], is shown in figure 1 and is clearly incompatible with the data. However a more refined calculation of Fredriksson *et al.* [22] which keeps SU(2) symmetry while relaxing SU(6) is in agreement with the data at large x, though it appears to deviate from it at lower x.

6. SUMMARY

Using the largest sample of data available for neutrino and antineutrino interactions on a pure hydrogen target we have measured the quark and antiquark structure functions of the proton within the framework of the quark parton model in the region of Bjorken x from 0 to 0.7. The valence quark distributions have been extracted and their ratio is compared with the predictions of quark-parton and diquark models. Models involving scattering from diquarks are in disagreement with the data.

ACKNOWLEDGEMENTS

We wish to thank the scanning and measuring teams at our laboratories for the careful attention our film received, and the staff at CERN for the operation of the SPS accelerator, neutrino beam, BEBC, the EMI and the IPF.

REFERENCES

[1] J. Aubert *et al.*, *Phys. Lett.* **123B** (1983) 275.

[2] A. Bodek *et al.*, *Phys. Rev. Lett.* **50** (1983) 1431;
A. Bodek *et al.*, *Phys. Rev. Lett.* **51** (1983) 534.

[3] G. Cavallari *et al.*, *IEEE Trans. on Nucl. Sci.*, Vol. **NS 25**, No.1 (1978) 600.

[4] M. Aderholz *et al.*, *Phys. Lett.* **173B** (1986) 211.

[5] C. Brand *et al.*, *Nucl. Instr. and Meth.* **136** (1976) 485;
R. Beuselinck *et al.*, *Nucl. Instr. and Meth.* **154** (1978) 445.

[6] H. Foeth, *Nucl. Instr. and Meth.* **176** (1980) 203.

[7] R. Voss, Proc. Int. Symposium on Lepton and Photon Interactions at High Energies, Hamburg (1987), p581.

[8] R. Giles, *D.Phil. Thesis*, Oxford, 1981.

[9] G. Corrigan, *D.Phil. Thesis*, Oxford, 1983.

[10] A. de Rujula *et al.*, *Nucl. Phys.* **B154** (1979) 394.

[11] H. Georgi and D. Politzer, *Phys. Rev.* **D14** (1976) 1829.

[12] H. Abramowicz *et al*, *Z. Phys.* **C25** (1984) 29.

[13] D. Allasia *et al*, *Z. Phys.* **C28** (1985) 321.

[14] F. Bobisut, Proc. Neutrino '84 Conference, Nordkirchen (1984), p422.

[15] R.D. Field and R.P. Feynman, *Phys. Rev.* **D15** (1977) 2590.

[16] G.R. Farrar and D.R. Jackson, *Phys. Rev. Lett.* **35** (1975) 1416.

[17] F.E. Close, *Phys. Lett.* **43B** (1973) 422.

[18] R. Carlitz, *Phys. Lett.* **58B** (1975) 345.

[19] F.E. Close and A.W. Thomas, *Phys. Lett.* **212B** (1988) 227.

[20] F.E. Close and R.G. Roberts, *Z. Phys.* **C8** (1981) 57.

[21] A. Donnachie and P.V. Landshoff, *Phys. Lett.* **95B** (1980) 437.

[22] S. Fredriksson *et al.*, *Z. Phys.* **C14** (1982) 35.

TABLE CAPTIONS

TABLE 1 Assumed values for $R(x)$ and $\alpha(x)$.

TABLE 2 Structure function $xq^{\nu}(x, Q_0^2)$ for $Q_0^2 = 14.2$ (GeV/c)^2.

TABLE 3 Structure function $xq^{\bar{\nu}}(x, Q_0^2)$ for $Q_0^2 = 8.6$ (GeV/c)^2.

TABLE 4 Structure function $x\bar{q}^{\bar{\nu}}(x, Q_0^2)$ for $Q_0^2 = 8.6$ (GeV/c)^2.

TABLE 5 Structure functions xd_v, xu_v and the ratio d_v/u_v.

Figure Caption

The results for the ratio d_v/u_v at $Q^2 = 11.5$ (GeV/c)^2. The solid bars indicate statistical errors and the dotted bars total errors. An overall error of 6% due to the relative uncertainties of the ν and $\bar{\nu}$ total cross sections is not included. Also shown are the predictions of an SU(6) symmetry breaking model [17,18] with two values of the parameter a — (dashed curves); the model of ref.19 with two values of the bag radius R — (dotted curves); the diquark model of ref.20 — (solid curve); the diquark model of ref.22 — (dashed-dotted curve); the QCD-based calculation of ref.16.

TABLE 1

x	0 – 0.1	0.1 – 0.2	0.2 – 0.3	0.3 – 0.4	0.4 – 0.5	0.5 – 0.6	0.6 – 0.7
R	0.28	0.10	0.05	0.02	0.01	0	0
α	0.08	−0.01	−0.06	−0.09	−0.11	−0.14	−0.18

TABLE 2

x interval	0.0–0.1	0.1–0.2	0.2–0.3	0.3–0.4	0.4–0.5	0.5–0.6	0.6–0.7
$xq^{\nu}(x, Q_0^2)$	0.409	0.330	0.253	0.205	0.115	0.063	0.023
Stat. error	0.020	0.013	0.011	0.006	0.004	0.003	0.002
Error due to flux shape uncertainty	0.002	0.001	–	–	–	–	–
Error due to change of α of 0.05	+0.014	+0.007	−0.010	+0.001	–	–	–
Error due to 25% increase in $R(x)$	−0.001	−0.002	–	–	–	–	–
Error due to smearing factors	0.009	0.007	0.012	0.010	0.012	0.006	0.002
Total systematic error excluding flux normalization	0.017	0.010	0.016	0.010	0.012	0.006	0.002

TABLE 3

x interval	0.0–0.1	0.1–0.2	0.2–0.3	0.3–0.4	0.4–0.5	0.5–0.6	0.6–0.7
$xq^{\bar{\nu}}(x,Q_0^2)$	0.569	0.663	0.720	0.678	0.534	0.337	0.148
Stat. error	0.100	0.051	0.039	0.025	0.023	0.018	0.011
Error due to flux shape uncertainty	0.022	0.008	0.008	0.009	0.005	0.008	0.003
Error due to change of α of 0.05	+0.050	+0.007	+0.023	+0.010	+0.006	–	–
Error due to 25% increase in $R(x)$	−0.041	−0.013	−0.019	+0.001	−0.011	–	–
Error due to smearing factors	0.027	0.055	0.059	0.034	0.053	–	0.015
Total systematic error excluding flux normalization	0.073	0.058	0.067	0.037	0.054	0.008	0.015

TABLE 4

x interval	0.0 – 0.1	0.1 – 0.2	0.2 – 0.3
$x\bar{q}^{\bar{\nu}}(x, Q_0^2)$	0.209	0.120	0.035
Stat. error	0.026	0.014	0.010
Error due to flux shape uncertainty	0.002	0.001	–
Error due to change of α of 0.05	−0.003	+0.014	−0.004
Error due to 25% increase in $R(x)$	−0.007	−0.004	−0.001
Error due to smearing factors	0.013	0.006	0.006
Total systematic error excluding flux normalization	0.015	0.016	0.007

TABLE 5

x interval	xd_v	xu_v	d_v/u_v
0.0–0.1	$0.189 \pm 0.033 \pm 0.023$	$0.617 \pm 0.116 \pm 0.073$	$0.306 \pm 0.107 \pm 0.052$
0.1–0.2	$0.211 \pm 0.019 \pm 0.019$	$0.524 \pm 0.062 \pm 0.058$	$0.402 \pm 0.075 \pm 0.057$
0.2–0.3	$0.222 \pm 0.015 \pm 0.018$	$0.656 \pm 0.047 \pm 0.067$	$0.338 \pm 0.040 \pm 0.044$
0.3–0.4	$0.209 \pm 0.006 \pm 0.010$	$0.660 \pm 0.025 \pm 0.037$	$0.316 \pm 0.015 \pm 0.023$
0.4–0.5	$0.117 \pm 0.004 \pm 0.012$	$0.517 \pm 0.023 \pm 0.054$	$0.226 \pm 0.013 \pm 0.033$
0.5–0.6	$0.065 \pm 0.003 \pm 0.006$	$0.324 \pm 0.018 \pm 0.009$	$0.200 \pm 0.015 \pm 0.019$
0.6–0.7	$0.024 \pm 0.002 \pm 0.002$	$0.141 \pm 0.011 \pm 0.015$	$0.169 \pm 0.018 \pm 0.023$

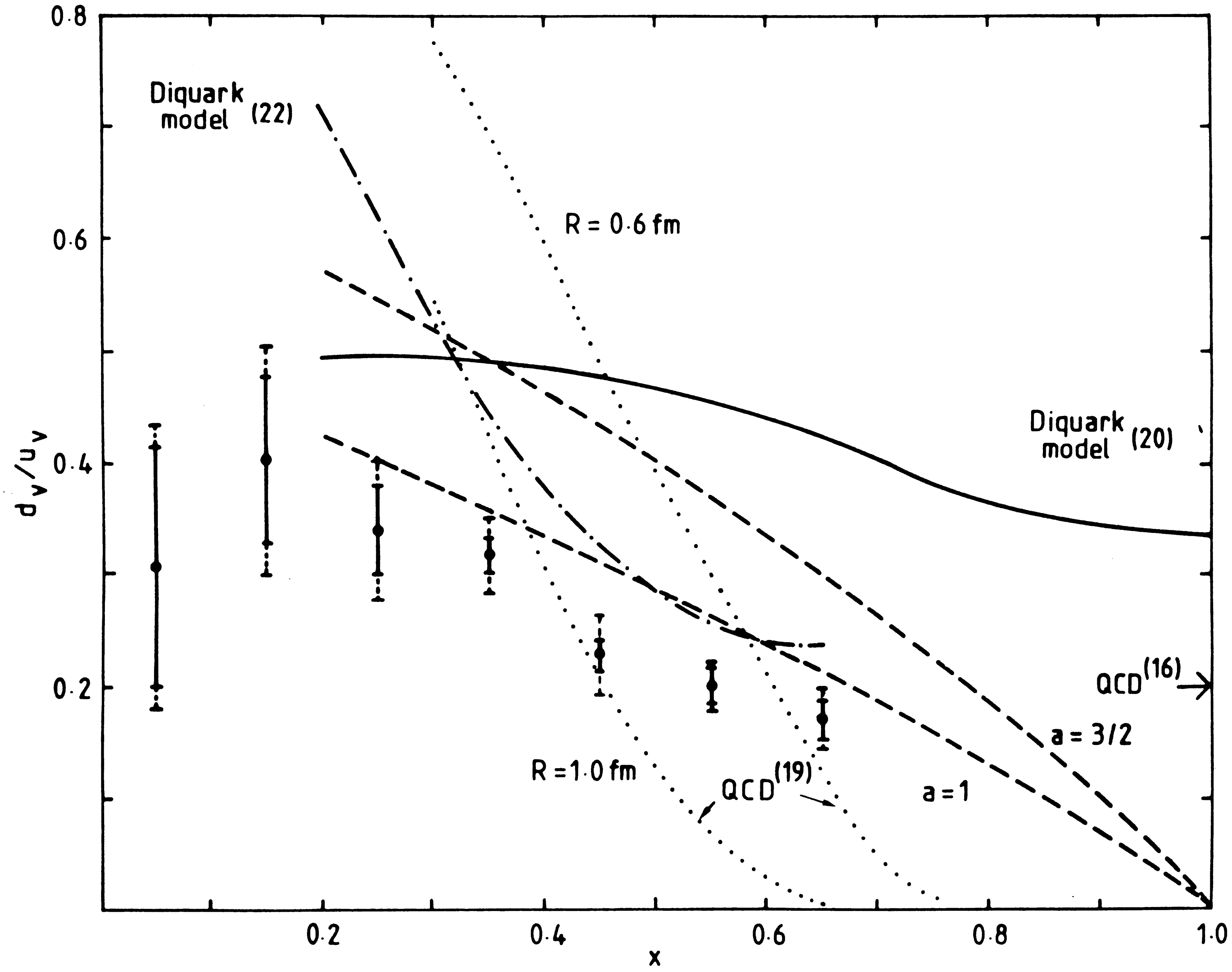

0·8
0·6
0·4
0·2
d_v/u_v
0·2
0·4
0·6
0·8
1·0
x
Diquark model (22)
Diquark model (20)
R = 0·6 fm
R = 1·0 fm
QCD(19)
QCD(16)
a = 3/2
a = 1